165 (2021) 203656

Contents lists available at ScienceDirect

Cells & Development

journal homepage: www.journals.elsevier.com/cells-and-development

Dysregulation of Rho GTPases in orofacial cleft patients-derived primary cells leads to impaired cell migration, a potential cause of cleft/lip palate development

Mirvat El-Sibai [a], Joelle El Hajj [a], Maria Al Haddad [a], Nada El Baba [a], Mounir Al Saneh [a], Wassim Daoud Khatoun [a], Raphaël Helaers [c], Miikka Vikkula [c], Oula El Atat [a], Joseph Sabbagh [b], Naji Abou Chebel [d], Michella Ghassibe-Sabbagh [a,*]

[a] Department of Natural Sciences, School of Arts and Sciences, Lebanese American University, Beirut, Lebanon
[b] Department of Restorative Dentistry and Endodontics, Faculty of Dental Medicine, Lebanese University, Beirut, Lebanon
[c] Laboratory of Human Molecular Genetics, de Duve Institute, University of Louvain, Brussels, Belgium
[d] Department of Otolaryngology - Head and Neck Surgery, Faculty of Medicine, American University of Beirut, Beirut, Lebanon

ARTICLE INFO

Keywords:
Cleft lip/palate
Rho GTPases
Motility
Mutation

ABSTRACT

Cleft lip and/or palate are a split in the lip, the palate or both. This results from the inability of lip buds and palatal shelves to properly migrate and assemble during embryogenesis. By extracting primary cells from a cleft patient, we aimed at offering a better understanding of the signaling mechanisms and interacting molecules involved in the lip and palate formation and fusion. With Rho GTPases being indirectly associated with cleft occurrence, we investigated the role of the latter in both. First, whole exome sequencing was conducted in a patient with cleft lip and palate. Primary fibroblastic cells originating from the upper right gingiva region were extracted and distinct cellular populations from two individuals were obtained: a control with no cleft phenotype and a patient with a cleft lip and palate. The genetic data showed three candidate variables in *ARHGEF18*, *EPDR1*, and *CUL7*. Next, the molecular data showed no significant change in proliferation rates between healthy patient cells and CL/P patient cells. However, CL/P patient cells showed decreased migration, increased adhesion and presented with a more elongated phenotype. Additionally, RhoA activity was upregulated in these cells, whereas Cdc42 activity was downregulated, resulting in loss of polarity. Our results are suggestive of a possible correlation between a dysregulation of Rho GTPases and the observed phenotype of cleft lip and palate patient cells. This insight into the intramolecular aspect of this disorder helps link the genetic defect with the observed phenotype and offers a possible mechanism by which CL/P occurs.

1. Introduction

Non-syndromic cleft lip and/or palate (NSCL/P) is a complex multifactorial disorder considered one of the most common congenital malformations (Bueno et al., 2011). Although not a major cause of mortality in developed countries, NSCL/P does cause considerable morbidity in affected children (Dixon et al., 2011). As a sub-phenotype of non-syndromic orofacial clefts (OFCs), NSCL/P affects 1 in 700 births and is considered the most common congenital craniofacial birth defect (Christianson et al., 2005; Zeiger et al., 2002). It results from a failure in the lip buds and/or palatal shelves to properly position, proliferate, migrate and fuse (Setó-Salvia and Stanier, 2014).

The development of the lip and palate during embryogenesis requires a tightly regulated multistep process involving -but not limited to- cellular proliferation, adhesion and motility (Houweling et al., 2009). Of these, cell motility is a vital function for a vast range of physiological processes, including the aforementioned, wound healing, embryogenesis, inflammatory response, and tissue engineering (Hanna and El-

* Corresponding author at: Department of Natural Sciences, Lebanese American University, P.O. Box: 13-5053, Chouran 1102 2801 Beirut, Lebanon.
E-mail addresses: mirvat.elsibai@lau.edu.lb (M. El-Sibai), joelle.elhajj@lau.edu.lb (J. El Hajj), maria.alhaddad@lau.edu (M. Al Haddad), nada.elbaba@lau.edu (N. El Baba), mounir.alsaneh@lau.edu.lb (M. Al Saneh), wassim.daoudkhatoun@lau.edu (W. Daoud Khatoun), raphael.helaers@uclouvain.be (R. Helaers), miikka.vikkula@uclouvain.be (M. Vikkula), oula.elatat@lau.edu.lb (O. El Atat), josephsabbagh@ul.edu.lb (J. Sabbagh), naji.abou-chebel@aub.edu.lb (N. Abou Chebel), michella.sabbagh@lau.edu.lb (M. Ghassibe-Sabbagh).

https://doi.org/10.1016/j.cdev.2021.203656
Received 20 August 2020; Received in revised form 24 November 2020; Accepted 25 November 2020
Available online 8 February 2021

Sibai, 2013; Lauffenburger and Horwitz, 1996; Najm and El-Sibai, 2014; Saykali and El-Sibai, 2014). Generally, eukaryotic cells identify chemical and physical signals from their surroundings and convert them into a multiplied intercellular signal that guides actin polymerization in a process called chemotaxis (Saykali and El-Sibai, 2014; Wang et al., 2011). Cells receive an extracellular signal to which they form a polarized protrusion at the leading edge. The protrusion adheres to the underlying extracellular matrix (ECM). Contraction of the cell body pushes the cell forward. Finally, the cell de-adheres at the trailing end and retracts its tail, moving forward (Bravo-Cordero et al., 2013b).

Rho GTPases regulate the actin cytoskeleton in the previously mentioned cellular processes (Khalil and El-Sibai, 2012). These are signal transducers that contribute to many essential pathways within the cell including, but not limited to, gene expression, cellular motility, adhesion and proliferation (Nasrallah et al., 2014; Spiering and Hodgson, 2011). Due to their GTPase characteristics, they serve as molecular switches. When bound to GTP, Rho GTPases are active. However, when they are bound to GDP, they become inactive. When active, Rho GTPases, in turn, activate downstream proteins, undergoing GTP hydrolysis and becoming inactive (El Baba et al., 2020; Gibbs et al., 1990).

Both environmental and genetic factors and the interactions between the two have been implied in the etiology of the NSCL/P malformation. Genetic factors, including aberrant gene variants inherited from either parents, may be directly responsible for NSCL/P or may confer a susceptibility to an increased risk of developing a cleft (Setó-Salvia and Stanier, 2014). Numerous genes have been shown to be mutated in syndromic forms of clefts, such as *IRF6*, a gene mutated in Van der Woude syndrome (VWS; OMIM #119300), the most common form of syndromic clefting. Kabuki, Miller, and Bartsocas-Papas cleft syndromes had their etiology unraveled through exome sequencing with mutations identified in KMT2D, DHODH, and RIPK4 respectively (Leslie and Marazita, 2013). Despite recent advances, the etiology of the genetically complex NSCL/Ps is still not fully understood. Genes such as FAF1, SUMO1, SATB2, and FGFR1 has been shown to be associated with NSCL/Ps in different populations (Alkuraya et al., 2006; Ghassibe-Sabbagh et al., 2011; Kim et al., 2005).

Recently, Rho GTPases have been indirectly associated with cleft occurrence. The Wnt signaling pathway, known to cause OFCs, meet Rho GTPases as RhoA acts downstream of multiple Wnt signaling molecule (Zhu et al., 2006). Syndromic and non-syndromic OFCs have been attributed to mutations in several WNT signaling molecules such as PORCN, an acyltransferase that modifies nascent WNT proteins shown to be mutated in Goltz–Gorlin syndrome, which includes orofacial clefts (Lombardi et al., 2011). Multiple coding and non-coding single nucleotide polymorphisms (SNPs) in WNT3, WNT6-WNT10A cluster, as well as WNT7A were associated with either CL/P or CPO (Reynolds et al., 2019). In addition, mutations in various Wnt signaling genes were shown to cause OFCs in animal models (He and Chen, 2012). *P63*, the gene responsible for anomalies such as ectrodactyly, ectodermal dysplasia, and facial clefting, is a Wnt target that regulates cellular proliferation and differentiation (Truong et al., 2006). *P63* is suggested to activate *IRF6*, the gene responsible for van der Woude, the most common cleft syndrome (Ghassibé et al., 2004). IRF6 signals upstream of Arhgap29, a cleft-associated Rho GTPase, regulating Rho activity downstream of Wnt5a (Leslie et al., 2012). The Rho guanine nucleotide exchange factor 2 (ARHGEF2) was shown to be mutated in two boys with craniofacial dysmorphism and high palate. ARHGEF2 disruption reduces the activity of the RhoA/ROCK/MLC, a major cell migration pathway (Ravindran et al., 2017). This further solidifies the potential defect in migration as a cause of cleft occurrence. This also suggests a potential correlation between cleft occurrence and the dysregulation of Rho GTPases.

Accordingly, in this study we examined the migration profile of primary cells taken from cleft patients and compared that to control cells. Indeed, our data has shown that the DNA extracted from a sporadic cleft patient harbors nucleotide changes in *ARHGEF18*, *CUL7*, and *EPDR1* genes, which are involved in cell adhesion and migration. We then directly studied the migratory ability of the cleft cells, their adhesion characteristics, as well as the activation status of Rho GTPases in these cells, in order to elucidate the mechanism of this birth defect.

2. Results

2.1. Subject clinical phenotype and WES results

The index was a 14-year old girl born with a unilateral, left-sided, cleft lip and palate. She was born to healthy parents without a family history of cleft. Although no consanguineous marriage was noted, the couple had a second child presenting with an orofacial phenotype (medical data and DNA not available). Whole exome sequencing analysis of the proband using the most stringent criteria generated a list of 111 candidate variants (Supplemental Table S1). The comparison of these variants to the list of 4274 "cleft lip and palate" genes generated by GeneCards, followed by an extensive search of the literature and the functional implication of the variants in orofacial development in human as well as animal models led to the retention of three variables in different candidate genes: *ARHGEF18*, *EPDR1*, and *CUL7* (Table 1). The G > A transition in *ARHGEF18* leads to a p.Arg495Gln amino acid change. This variant, with a CADD score of 28.1, is reported in gnomAD with an allele frequency of 8.05×10^{-5}. The p.Val102Ala detected in *EPDR1* has a CADD score of 26.7 and is reported in the dbSNP as rs374633177. It has an allele frequency of 1.84×10^{-4} in gnomAD. The C > T transversion in *CUL7* with a CADD score of 16, leads to a p.Pro945Ser substitution present in gnomAD with an allele frequency of 3.32×10^{-4}. The protein sequences alignment of ARHGEF18, EPDR1 and CUL7 with their respective sequences of nine species representative of mammalians and non-mammalians showed that the three substitutions affect amino acids that are conserved across species (Supplemental Fig. S1). In addition, Secondary structure analysis of the wild-type versus mutated proteins using Phyre2 showed that the mutation in ARHGEF18 is speculated to disrupt a beta sheet secondary structure of the protein (Supplemental Fig. S1).

2.2. Difference in proliferation rate between healthy cells and cleft patient cells

Healthy and cleft cells appeared to have a comparable rate of proliferation/growth in culture (Fig. 1A). A WST-1 proliferation assay was performed on healthy and cleft cells to see if there would be a difference in proliferation rate that can explain the abnormal phenotype. Results of the WST-1 assay showed a slight increase in the proliferation rate of the patient cells; however this increase was not significant (Fig. 1B). Therefore, the defect could not be attributed to this rate.

2.3. Cellular migration rate difference in cleft patient cells

Since no difference was observed in proliferation, we next looked at the migration of the cells. To study both cellular lines' motility, wound healing assays were performed. Cell lines were allowed to grow in normal serum medium in monolayers. Results showed a decrease in cell migration of patient cells, TCF5 cells, in comparison with the TCF3 healthy donor cells. This effect is shown by a significant decrease in the rate of wound closure at 72 h (Fig. 2A and B). We also performed a single cell 2D random migration in serum assay, in order to eliminate the proliferation component (which might play an additional role in the wound healing difference). A motility assay was performed to evaluate motility in 2D (Fig. 2C, D and E, as well as Supplemental movies S1 and S2). A significant decrease in cellular migration in cleft patient cells was observed. The cleft patient cells had a decrease in net path as they underwent random migration in serum (26 μm in the patient cells compared to approximately 51 μm in healthy cells). This decrease in motility could be the driving force behind the defect. Hence, we wanted

Table 1
Variants passing specific analysis filter in WES data.

Chr	BP	RA	AA	Gene	Protein change	DNA change	dbSNP	AA freq	SnpEff	SIFT	Pph2	LRT	Mut taster	Cadd
19	7,518,545	G	A	ARHGEF18	p.Arg495Gln	c.1484G>A	rs779040030	0.00008	NS	DA	PD	D	DC	28.1
7	37,988,477	T	C	EPDR1	p.Val102Ala	c.305T>C	rs374633177	0.00018	NS	T	B	D	DC	26.7
6	43,014,053	G	A	CUL7	p.Pro945Ser	c.2833C>T	rs147452416	0.00033	NS	DA	B	D	DC	16.79

For each variant we give the gene name, chromosome (Chr), base pair (BP), reference allele (RA), alternate allele (AA), protein change, DNA change, the ID in dbSNP, the frequency of the AA for all populations in GnomaD, functional effect prediction according to the following programs: SnpEff, Pholyphen2 score based on HVAR (pph2), LRT prediction (LRT), MutationTaster prediction (Mut taster), and CADD phred-like score (Cadd). B, benign; D, deleterious; DA, damaging; DC, disease causing; PD, probably damaging; T, tolerated.

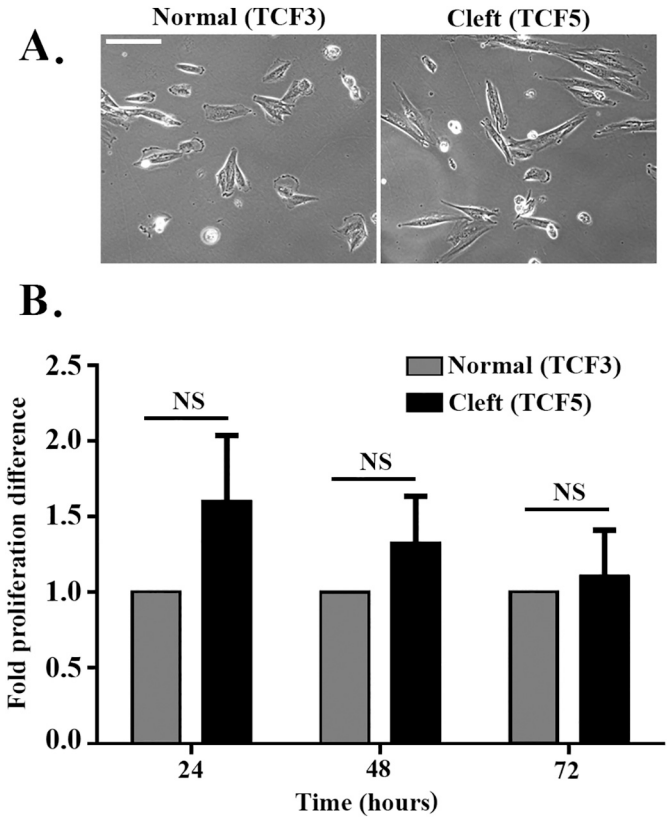

Fig. 1. Normal and cleft cells have similar cellular proliferation rates. (A) Representative micrographs (phase contrast) of normal (TCF3) and cleft (TCF5) grown in culture. The scale bar is 50 μm. (B) Tetrazolium salt (WST-1) was added to normal (TCF3) and cleft (TCF5) cells after 24, 48 and 72 h incubation and O.D. was measured using an ELISA plate reader at 450 mm. Results are the quantitation of three different experiments using two way ANOVA statistical test with post-hoc Tukey of the image J software, and expressed as the fold change to control. Data are the mean ± SEM. $P < 0.05$ (ns $P > 0.05$) indicates a statistically significant difference.

to check next if the decrease in motility was due to an increase in the adhesion of cells to their ECM.

2.4. Cellular adhesion is greater in cleft patient cells compared to healthy cells

Cells were plated on collagen to test for their adhesion. As seen in Fig. 3A and B, cleft patient cells showed an increase in adhesion. Knowing that cells need to release their adhesion at the tail in order to retract and move forward (Bravo-Cordero et al., 2013a), the increased adhesion might explain the decreased migratory ability of these cells. Indeed, when cells were immunostained for vinculin, a marker for focal adhesions, cleft patient cells appeared to have persistent focal adhesions at the tail (Fig. 4). This might explain the elongated phenotype observed in these cells as well as their decreased motility due to their potential inability to detach at the tail (Supplemental movie S2 and Fig. 1A).

2.5. Increased RhoA activation in cleft patient cells consistent with increased adhesion

Since RhoA is a known regulator of focal adhesions, we next investigated if the increase in focal adhesions was regulated by an increase in RhoA activity. RhoA activation levels were assessed using the previously described RhoA biosensor in healthy cells and in cleft patient cells (Pertz et al., 2006). Both cell lines were imaged for RhoA activation in the FRET channel and the FRET image was ratioed to total expression of the RhoA biosensor. Consistently with the increase in adhesion, cleft patient cells had an increased RhoA activation (Fig. 5A and B).

2.6. Loss of cellular polarity due to decrease in Cdc42 activation in cleft patient cells

Additionally, in an attempt to explain the loss of polarity of the cleft patient cells, Cdc42 activation levels were studied. Similarly, cells were transfected with a Cdc42 FRET biosensor (Hanna et al., 2014). Cleft patient cells showed a significant decrease of approximately two folds in Cdc42 activation, which explains the loss of polarity of these cells (Fig. 5C and D).

3. Discussion

We used the whole exome technology to address the pathogenesis of isolated cleft lip and palate. We found that rare variants in *ARHGEF18*, *EPDR1*, and *CUL7* might explain the phenotype. Although these variants are present in the general population, their low reported incidence together with the polygenic nature of clefts might explain the fact that each variant contributes to a small impairment of cellular adhesion and migration, summing in a cell that loses its polarity and its ability to migrate towards the chemoattractant.

Due to the role Rho GTPases play in cellular motility and migration, we hypothesized that a dysregulation in these GTPases could be the underlying cause in development of cleft lip and/or palate. Of the 20 known Rho GTPases, the most prominent and widely studied are RhoA and Cdc42. The orofacial region develops from cells that are polarized along the apicobasal axis. Loss of this polarity results in abnormal organ architecture, morphology and proliferation (Groeger and Meyle, 2019). We found that variants in ARHGEF18, a RhoA and Rac1 guanine nucleotide exchange factor (GEF), affect apicobasal polarity of the cells derived from the orofacial region of a cleft lip and palate patient (Blomquist et al., 2000; Nagata and Inagaki, 2005; Niu et al., 2003). RhoA regulates tight junction assembly, cortical actin cytoskeleton and apicobasal polarity but its functional relevance for orofacial development has not been addressed so far (Nakajima and Tanoue, 2011; Terry et al., 2011). RhoA is known to control focal adhesion dynamics via ROCK whereby when the cell adheres to the ECM, RhoA gets activated (Hernández et al., 2004; Khalil et al., 2014). It recruits actin to initiate the formation of early stage adhesions. If these temporary adhesions mature into focal adhesions, the cell becomes fixed to the ECM and

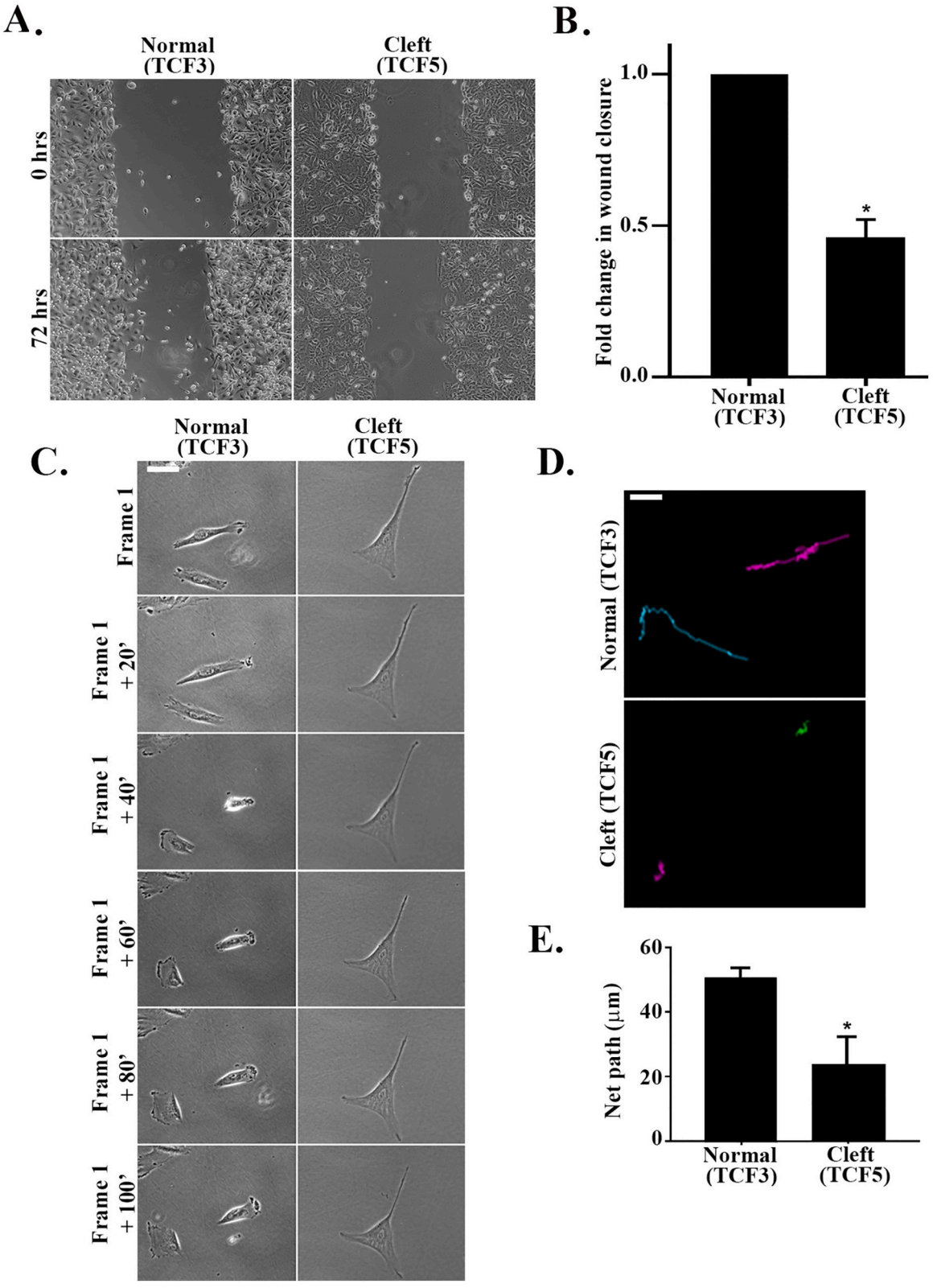

Fig. 2. Cleft cells present lower motility compared to normal cells.
Cell monolayers were wounded and images were taken at time 0 and 72 h. (A) Representative wound closure images of normal (TCF3) and cleft (TCF5) cells. The scale bar is 100 μm. (B) Frames were quantitated using Image J (National Institutes of Health, MA, USA). The width of each wound was measured at 13 different points. The average rate of wound closure was calculated and expressed as μm/h. (C) Cell monolayers were plated on petri dishes and images every 1 min for 2 h at 20×. Representative micrographs of normal (TCF3) and cleft (TCF5) cells undergoing migration in serum. The frames shown are separated by 20 min. The scale bar is 50 μm. (D) Representative net path micrographs. The scale bar is 50 μm. (E) Quantitation of the net path of migration fold in cleft (TCF5) cells normalized to the control (TCF3), of 120 frames from time lapse movies of cells with an overall duration of 2 h displaying random cell motility in serum. Data are the mean ± SEM taken from 10 randomly selected cells for each condition. Data are the mean ± SEM. $P < 0.05$ ($^*P < 0.05$) indicates a statistically significant difference.

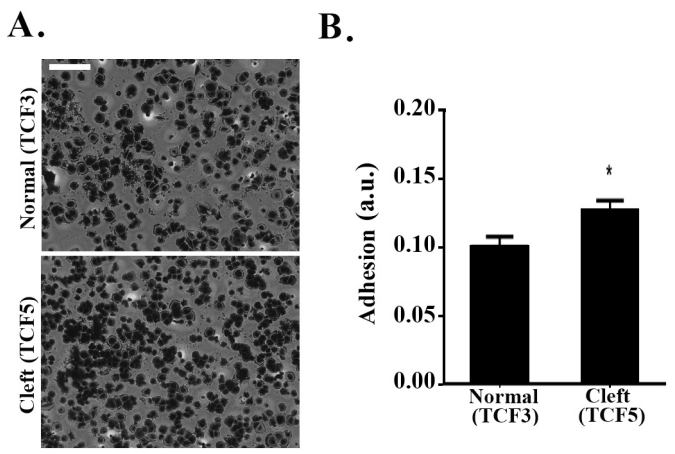

Fig. 3. Cleft cells have greater adhesion to collagen compared to normal cells. (A) Representative micrographs of normal (TCF3) and cleft (TCF5) cells plated, fixed and stained with crystal violet as described in the Materials and methods. The scale bar is 100 μm. (B) Quantitation of (A). Absorption of the solubilized crystal violet was measured at 550 nm using an ELISA plate reader. Data are the mean ± SEM. $P < 0.05$ ($^*P < 0.05$) indicates a statistically significant difference.

migration is halted.

Upon the occurrence of the latter, the activity of RhoA surges (Hernández et al., 2004; Salloum et al., 2020). As for Cdc42, through its WAVE-dependent activation of Arp2/3, it guides the polarity of actin polymerization and cell migration (Al-Koussa et al., 2020; Eden et al., 2002; Faour et al., 2018; Jaafar et al., 2020; Sadok and Marshall, 2014; Zohrabian et al., 2009). Although ARHGEF18 is not a RhoGEF for Cdc42 (Blomquist et al., 2000), RhoA activity has been shown to exert an effect on the activity of Cdc42 on its own (Guilluy et al., 2011; Salloum et al., 2020; Wennerberg et al., 2003).

As the activation of RhoA and Cdc42 is required to maintain a proper polarity of the cell, we speculated that ARHGEF18 mutation might lead to a dysregulation of RhoA activation explaining the adhesion and loss of polarity phenotype seen in the cells derived from the patient. As expected, the activity of RhoA was elevated in cleft patient cells in comparison to normal cells given their increased adhesion. Additionally, our cleft patient cells displayed a significant decrease in overall Cdc42 activation, which complements the loss of polarity and multidirectional protrusions observed in these cells. Previously, mutations of ARHGEF18 were shown to affect apicobasal polarity of the retinal neuroepithelium in medaka fish (Herder et al., 2013). In addition, a homozygous mutation in ARHGEF2 was shown to cause craniofacial dysmorphism and high palate in a family (Ravindran et al., 2017).

A second variant was found in *EPDR1* (ependymin related 1), a gene encoding a transmembrane protein involved in cell adhesion (Shashoua, 1991). It was early suggested that its extracellular domain might display antiadhesive properties (Hoffmann and Schwarz, 1996). Whether our variant leads to a decrease of EPDR1 function and thus explain the increased adhesion is warrant further investigation. Interestingly, diseases associated with EPDR1 include Weaver Syndrome that is characterized by the presence of occasional cleft lip and palate (Kunz et al., 2016).

The last candidate variant is present in *CUL7* associated with 3M syndrome. 3M syndrome is a severe recessive disorder characterized by short stature and unusual facial features with widespread skeletal abnormalities (Huber et al., 2009, 2005). CUL7 was shown to mediate degradation of RhoA to control actin cytoskeleton structure and cell

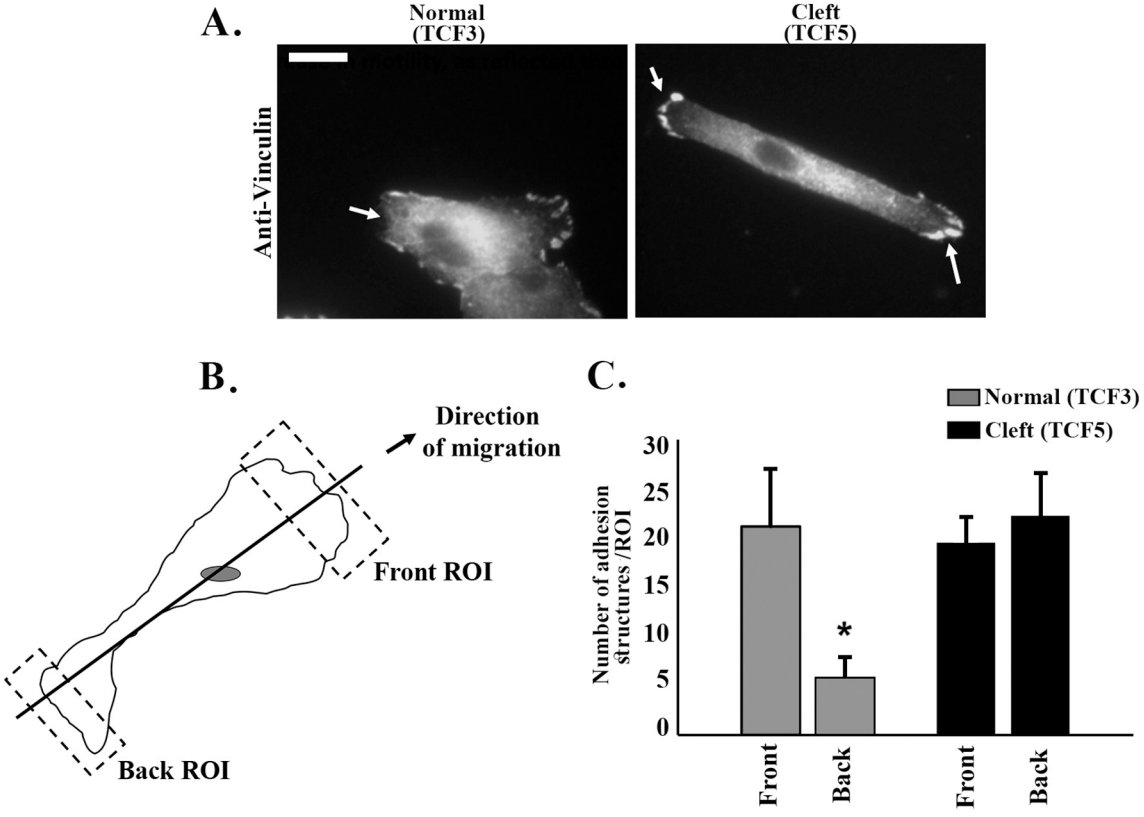

Fig. 4. Adhesion phenotypes of normal and cleft cells. (A) Representative micrographs of normal (TCF3) and cleft (TCF5) cells that were fixed and stained with anti-vinculin. Cells were imaged using a 60× objective. The scale bar is 10 μm. (B) Suggested model of phenotype in parallel with direction of migration. (C) Quantitation of focal adhesions. Results are the quantitation of three different experiments using statistical *t*-test of the image J software. Data are the mean ± SEM. $P < 0.05$ ($^*P < 0.05$) indicates a statistically significant difference.

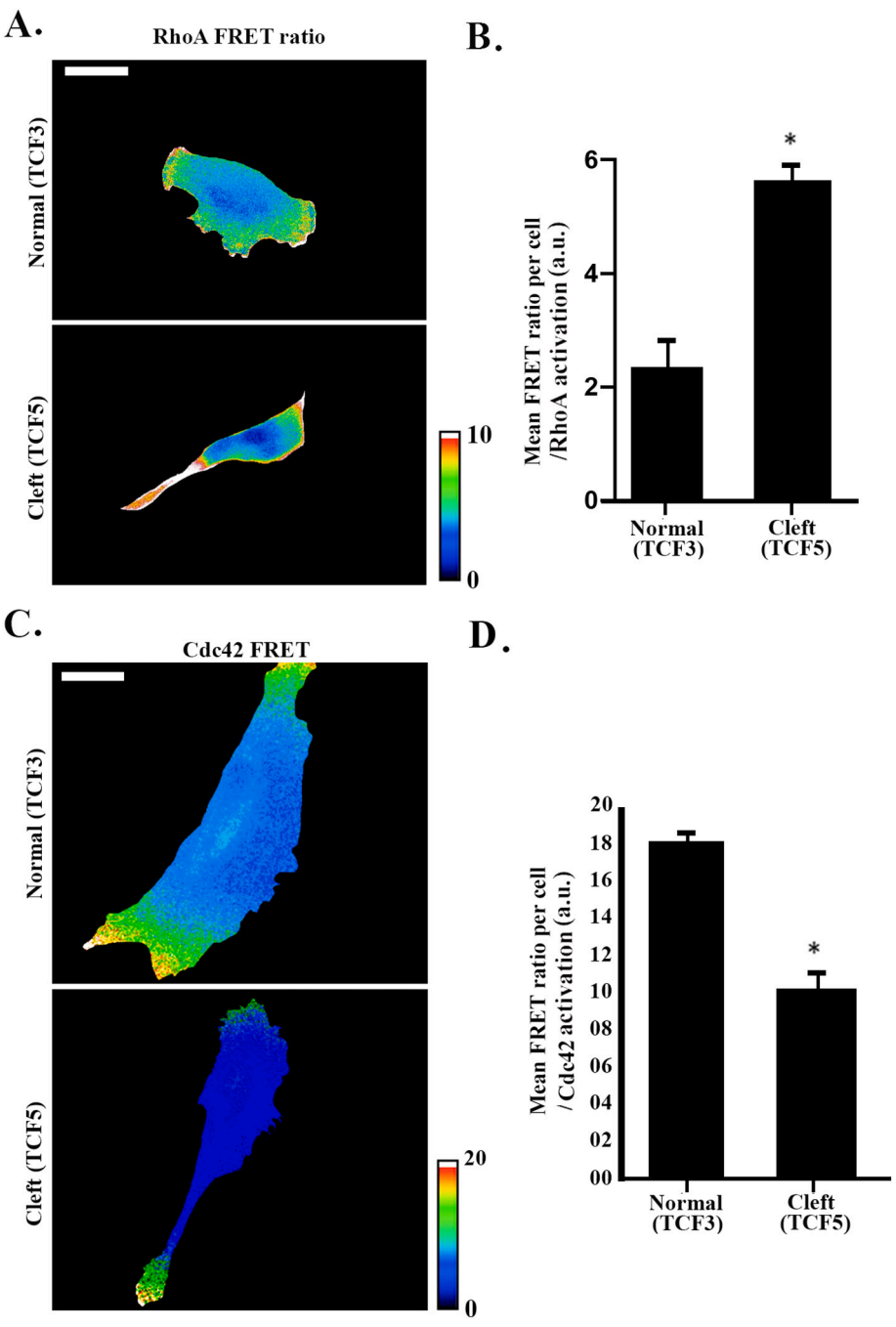

Fig. 5. Difference in RhoA and Cdc42 activation levels between normal and cleft cells. (A) Representative micrographs of normal (TCF3) and cleft (TCF5) cells that were transfected with the FRET RhoA biosensor. The cells were imaged using the FRET channel and the raw FRET images were normalized to the CFP images. The images reflect the FRET ratio = Raw FRET image/CFP. (B) The average intensity rate was quantified using ImageJ. (C) Representative micrographs of normal (TCF3) and cleft (TCF5) cells that were transfected with the FRET Cdc42 biosensor. The cells were imaged using the FRET channel and the raw FRET images were normalized to the CFP images. The images reflect the FRET ratio = Raw FRET image/CFP. (D) The average intensity rate was quantified using ImageJ. Data are the mean ± SEM. $P < 0.05$ ($^*P < 0.05$) indicates a statistically significant difference.

movement (Chen et al., 2009). A decrease in CUL7 function due to the present variation may contribute to the increase in RhoA seen in our patient phenotype.

In conclusion, our results have shown candidate variants in the *ARHGEF18*, *EPDR1*, and *CUL7* genes in the genomic DNA in a cleft patient. With *ARHGEF18* being described as a RhoGEF, a variant in this gene has caused a decrease in RhoA activity and subsequently resulted in a less motile, more adhesive phenotype. With RhoA exerting an indirect effect on Cdc42, the activation of the latter was upregulated resulting in a loss of polarity of the CL/P patient cells. Our data offers a clearer understanding of the genetic, molecular and phenotypic correlation underlying the development of CL/P, suggesting that a variant in the aforementioned genes dysregulates normal cellular processes resulting in the anomaly.

4. Materials and methods

4.1. Study subject and screening

Parents of a 14-years old girl who presented with a cleft lip and palate provided a written declaration of consent, prior to filling the questionnaire, as they were legally authorized representatives of their minor child. Research and data collection were carried out in compliance with the Helsinki Declaration, with the approval of the LAU Institutional Review Board and the Committee on Human Subjects in Research (CHSR). De-identified data about the neurological, muscular, epithelial, and connective tissues related development were obtained from the medical chart. Physical examination was conducted by two ascertained physicians.

We obtained a blood sample of two collection tubes (4–6 ml/tube).

Genomic DNA was extracted from peripheral blood of the participant using the standard phenol-chloroform extraction procedure.

4.2. Whole exome sequencing

WES was carried out by using 1 μg of genomic DNA. Whole exome enrichment was performed on genomic DNA using the SureSelect Human All Exon V6 (Agilent). WES was performed on an Illumina Hi-Seq 3000 platform using a 150 bp paired-end protocol with an average depth of 60×. Reads were aligned against the human assembly GRCh37 using Burrows-Wheeler Aligner (BWA). Data analysis was performed using SAMtools, Picard, the Genome Analysis Toolkit (GATK) and Variant Effect Predictor (VEP). Called variants were annotated, filtered, and visualized using Highlander (http://sites.uclouvain.be/highlander/), an in-house bioinformatics framework.

4.3. Classification and selection of variants identified by WES

Variants were retained if they passed quality criteria (Phred score for quality of mapping >30, no more than two different haplotypes at the considered position, variant called outside the 3′ end of the supporting reads, absence of strand bias), had an allele frequency of <0.001 in the Greater Middle East (GME) Variome project, gnomAD and in ExAC database, and were considered highly or moderately damaging by at least three out of eight prediction softwares (SIFT, CADD, FATHMM, LRT, DEOGEN2, Mutation Assessor, Mutation Taster, and Polyphen2).

We compared the generated results to a list of 4274 CL/P candidate genes supplemented in the human gene database GeneCards (https://www.genecards.org/Search/Keyword?queryString=cleft%20lip%20palate). Polymorphisms were removed by reference to their population frequencies by searching for such mutations in genetic disease databases including OMIM (http://omim.org), HGMD (http://www.hgmd.cf.ac.uk/ac/index.php), ClinVar (https://www.ncbi.nlm.nih.gov/clinvar/), the database of the 1000 Genomes Project (http://www.1000genomes.org/), ESP6500 (http://evs.gs.washington.edu/EVS/), and ExAC (http://exac.broadinstitute.org). When variants passed the selection criteria, they were ranked relative to their function in orofacial development. The prioritization of genes was conducted using Pubmatrix (https://pubmatrix.irp.nia.nih.gov/) and GeneCards (www.genecards.org) followed by further assessment in relation to clinical characteristics.

4.4. Primary cell culture

Primary cells were extracted from the orofacial region of the proband during surgical palatal repair. In parallel, a tissue biopsy was obtained from the upper right gingiva of a healthy 14 year-old girl. Tissues obtained from healthy and CL/P individuals were washed three times with PBS (Lonza) supplemented with 10% Penicillin Streptomycin Amphotericin (PSA) (Lonza). They were then cut into small pieces and plated into 6-well plates containing Dulbecco's modified Eagle's medium (Sigma) supplemented with 10% Fetal Bovine Serum (FBS) (Sigma) and 1% PS (Sigma) at 37 °C in the CO_2 incubator. After reaching confluence, fibroblasts were passaged subsequently in to T25 cm^2 and T75 cm^2 flasks and the medium was replaced every 3 days. At passage 3, cells were cryopreserved in liquid nitrogen. For the assays, fibroblasts were thawed, cultured, and expanded in T75cm^2 flasks containing DMEM (Sigma) supplemented with 10% FBS (Sigma) and 1% PS (Sigma) at 37 °C in the CO_2 incubator. All experiments were performed using passages 6–8. Normal healthy cells were labeled TCF3 and CL/P patient cells labeled TCF5.

4.5. Proliferation assay

Cells were seeded in a 96-well plate for 24 h, 48 h, and 72 h (Corning Inc. Corning, NY, USA). Cell viability was determined using water-soluble cell proliferation reagent WST-1 (Roche, Mannheim, Germany). After the addition of WST-1 for 2 h in a humidified incubator at 37 °C and 5% CO_2, the color change caused by the cleavage of the tetrazolium salt into formazan by mitochondrial dehydrogenases was measured using a Varioskan Flash plate reader at 450 mm (Thermo Fisher Scientific, Waltham, MA, USA).

4.6. Migration assays

4.6.1. Wound healing

Cells were grown to confluence on culture plates. After 24 h, a wound was made in the monolayer with a sterile pipette tip. Cells were then washed twice with PBS to remove debris and a new medium was added. Phase-contrast images of the wounded area were captured at 0 and 72 h after wounding. Wound widths were measured at 13 different points for each wound, and the average rate of wound closure was calculated (in μm/h) using the image J software. The assay was done using infinity-corrected optics on a Zeiss Observer Z1 microscope supplemented with a computer-driven Roper cooled CCD camera and operated by Zen software (Zeiss).

4.6.2. Time lapse

Cells were plated to confluence on culture plates. Motility assay was performed 2 h after seeding. For motility analysis, cells were imaged in *DMEM* (10% FBS, 1% Penstrep) media, buffered using HEPES, and overlaid with mineral oil on a 37 °C stage. Images were collected every 60 s for 2 h using a 20× objective lens on the Zeiss Observer Z1 microscope. The speed of cell movement was quantified using the ROI tracker plugin in the Image J software, which was used to calculate the total distance traveled by individual cells (Khalil et al., 2014). The speed is then calculated by dividing this distance by the time (120 min) and reported in μm/min. The speed of at least 10 cells for each condition was calculated. The net distance traveled by the cell was calculated by measuring the distance traveled between the first and the last frame.

4.7. Adhesion assay

96-well plates were coated with collagen using Collagen Solution, Type I from rat tail (Sigma) overnight at 37 °C then washed with a washing buffer (0.1% BSA in DMEM media). The plates were then blocked with 0.5% BSA in DMEM media at 37 °C in a CO_2 incubator for 1 h. This was followed by washing the plates and chilling them on ice. Meanwhile, the cells were trypsinized and counted to 4×10^5 cells/ml. 50 μl of cells were added in each well and incubated at 37 °C in a CO_2 incubator for 30 min. The plates were then shaken and washed 3 times. Cells were then fixed with 4% PFA at room temperature for 10 min, washed, and stained with crystal violet (5 mg/ml in 2% ethanol) for 10 min. Following the staining, the plates were washed extensively with water and left to dry completely. Crystal violet was solubilized by incubating the cells with 2% SDS for 30 min. The absorption of the plates was read at 550 nm using a Thermo scientific Varioskan Flash Multimode reader (Thermo Fisher Scientific, Waltham, MA, USA).

4.8. Immunocytochemistry and quantification of focal adhesions

Cells were plated on glass coverslips. They were fixed with 4% paraformaldehyde for 10 min at 37 °C and permeabilized with 0.5% Triton-X 10 for 15 min on ice. For blocking, cells were incubated with 1% filtered BSA in PBS for 1 h. Samples were then stained with primary antibodies anti-vinculin (Abcam) overnight at 4 °C and with fluorophore-conjugated secondary antibodies for 1 h. Fluorescent images were taken using a 63× objective lens on a Zeiss Observer Z1 microscope supplemented with a computer-driven Roper cooled CCD camera and operated by Zen software (Zeiss) and analyzed using Image J software. For focal adhesions quantifications, two main plugins of Image J software were used, CLAHE and Log3D. Briefly, CLAHE enhances the

local contrast of the image and Log3D filters the image based on user predefined parameters which allows detection and analysis of focal adhesions (Al-Koussa et al., 2020).

4.9. Fluorescence resonance energy transfer (FRET)

Healthy cells and cleft patient cells were transfected with 3 μg of either the RhoA or Cdc42 fluorescence resonance energy transfer (FRET)-based biosensor plasmids which shows an increase in FRET ratio with GTP loading of RhoA and Cdc42, using FuGENE (Promega) as described by the manufacturer. The RhoA biosensor consists of (from the n-terminus) the Rho binding domain (RBD) of the effector Rhotekin, a cyan fluorescent protein (CFP), a protease resistant 17-mer unstructured linker, a yellow fluorescent protein (YFP) domain, and a full-length RhoA. Activation of RhoA can be determined as a ratio of the FRET image over the CFP image. The Cdc42 biosensor constituted of mCer, followed by two p21 binding domains (PBD) from PAK1 linked to each other, trailed by mVenus linked to a full length Cdc42. FRET image sequences were obtained with an automated using a 63× objective lens on a Zeiss Observer Z1 microscope supplemented with a computer-driven Roper cooled CCD camera and operated by Zen software (Zeiss). A CFP/YFP FRET filter cube was used: YFP was imaged with exciter S500/20 and emitter S535/30 (YFP/acceptor image), CFP was imaged with exciter S430/25 and emitter S470/30 (CFP/donor image) or S535/30 (FRET image). Images were background corrected and the YFP images were thresholded to generate a binary mask with values of 1 within the cell and 0 for the background. This was used to remove the background from ratio calculations, by multiplying CFP and FRET images by the mask. The increase in FRET signal due to activation of RhoA and Cdc42 was detected by dividing the FRET image (CFP excitation- YFP emission) by the donor image (CFP excitation- CFP emission). FRET signals were quantified by averaging the mean FRET ratio in all the cell area and values were then normalized to control cells (untreated) and expressed as fold change (Khalil et al., 2014).

5. Statistical analysis

The results reported represent average values from three independent experiments. The error estimates are given as ± SEM. The *P*-values were calculated by a two-way ANOVA or *t*-test. The post hoc Tukey test was used for comparing all possible group pairings. $P < 0.05$ indicates statistically significant differences.

Supplementary data to this article can be found online at https://doi.org/10.1016/j.cdev.2021.203656.

CRediT authorship contribution statement

M. El-Sibai: reviewing and editing original draft, methodology, investigation
J. El Hajj: conceptualization, formal analysis
M. Al Haddad: writing, reviewing and editing draft, investigation
N. El Baba: investigation, formal analysis, visualization
M. Al Saneh: investigation, formal analysis, visualization
R. Helaers: formal analysis of the whole exome sequencing data
M. Vikkula: formal analysis of the whole exome sequencing data
O. El Atat: methodology, investigation, formal analysis, visualization
J. Sabbagh: data collection, formal analysis
N. Abou Chebel: data collection
M. Ghassibe-Sabbagh: reviewing and editing original draft, project administration, methodology, investigation, conceptualization.

Acknowledgments

This work was supported by the Natural Science Department at the Lebanese American University.

References

Al-Koussa, H., El Atat, O., Jaafar, L., Tashjian, H., El-Sibai, M., 2020. The role of Rho GTPases in motility and invasion of glioblastoma cells. Anal. Cell. Pathol. 2020, 9274016 https://doi.org/10.1155/2020/9274016.
Alkuraya, F.S., Saadi, I., Lund, J.J., Turbe-Doan, A., Morton, C.C., Maas, R.L., 2006. SUM01 haploinsufficiency leads to cleft lip and palate. Science (80-.). https://doi.org/10.1126/science.1128406.
Blomquist, A., Schwörer, G., Schablowski, H., Psoma, A., Lehnen, M., Jakobs, K.H., Rümenapp, U., 2000. Identification and characterization of a novel Rho-specific guanine nucleotide exchange factor. Biochem. J. 352, 319. https://doi.org/10.1042/0264-6021:3520319.
Bravo-Cordero, Jose Javier, Magalhaes, M.A.O., Eddy, R.J., Hodgson, L., Condeelis, J., 2013a. Functions of cofilin in cell locomotion and invasion. Nat. Rev. Mol. Cell. Biol. 14, 405–415. https://doi.org/10.1038/nrm3609.
Bravo-Cordero, J.J., Sharma, V.P., Roh-Johnson, M., Chen, X., Eddy, R., Condeelis, J., Hodgson, L., 2013b. Spatial regulation of RhoC activity defines protrusion formation in migrating cells. J. Cell Sci. 126, 3356–3369. https://doi.org/10.1242/jcs.123547.
Bueno, D.F., Sunaga, D.Y., Kobayashi, G.S., Aguena, M., Raposo-Amaral, C.E., Masotti, C., Cruz, L.A., Pearson, P.L., Passos-Bueno, M.R., 2011. Human stem cell cultures from cleft lip/palate patients show enrichment of transcripts involved in extracellular matrix modeling by comparison to controls. Stem Cell Rev. 7, 446–457. https://doi.org/10.1007/s12015-010-9197-3.
Chen, Y., Yang, Z., Meng, M., Zhao, Y., Dong, N., Yan, H., Liu, L., Ding, M., Peng, H.B., Shao, F., 2009. Cullin mediates degradation of RhoA through evolutionarily conserved BTB adaptors to control actin cytoskeleton structure and cell movement. Mol. Cell 35, 841–855. https://doi.org/10.1016/j.molcel.2009.09.004.
Christianson, A., H., C.P., M., B., 2005. March of Dimes: Global Report on Birth Defects, the Hidden Toll of Dying and Disabled Children.
Dixon, M.J., Marazita, M.L., Beaty, T.H., Murray, J.C., 2011. Cleft lip and palate: understanding genetic and environmental influences. Nat. Rev. Genet. 12, 167–178. https://doi.org/10.1038/nrg2933.
Eden, S., Rohatgi, R., Podtelejnikov, A.V., Mann, M., Kirschner, M.W., 2002. Mechanism of regulation of WAVE1-induced actin nucleation by Rac1 and Nck. Nature 418, 790–793. https://doi.org/10.1038/nature00859.
El Baba, N., Farran, M., Khalil, E.A., Jaafar, L., Fakhoury, I., El-Sibai, M., 2020. The role of Rho GTPases in VEGF signaling in cancer cells. Anal. Cell. Pathol. https://doi.org/10.1155/2020/2097214.
Faour, W.H., Fayyad-Kazan, H., El Zein, N., 2018. fMLP-dependent activation of Akt and ERK1/2 through ROS/Rho A pathways is mediated through restricted activation of the FPRL1 (FPR2) receptor. Inflamm. Res. 67, 711–722. https://doi.org/10.1007/s00011-018-1163-6.
Ghassibé, M., Revencu, N., Bayet, B., Gillerot, Y., Vanwijck, R., Verellen-Dumoulin, C., Vikkula, M., 2004. Six families with van der Woude and/or popliteal pterygium syndrome: all with a mutation in the IRF6 gene. J. Med. Genet. 41, e15 https://doi.org/10.1136/jmg.2003.009274.
Ghassibe-Sabbagh, M., Desmyter, L., Langenberg, T., Claes, F., Boute, O., Bayet, B., Pellerin, P., Hermans, K., Backx, L., Mansilla, M.A., Imoehl, S., Nowak, S., Ludwig, K. U., Baluardo, C., Ferrian, M., Mossey, P.A., Noethen, M., Dewerchin, M., François, G., Revencu, N., Vanwijck, R., Hecht, J., Mangold, E., Murray, J., Rubini, M., Vermeesch, J.R., Poirel, H.A., Carmeliet, P., Vikkula, M., 2011. FAF1, a gene that is disrupted in cleft palate and has conserved function in zebrafish. Am J Hum Genet 88, 150–161. https://doi.org/10.1016/j.ajhg.2011.01.003.
Gibbs, J.B., Marshall, M.S., Scolnick, E.M., Dixon, R.A., Vogel, U.S., 1990. Modulation of guanine nucleotides bound to Ras in NIH3T3 cells by oncogenes, growth factors, and the GTPase activating protein (GAP). J. Biol. Chem. 265, 20437–20442.
Groeger, S., Meyle, J., 2019. Oral mucosal epithelial cells. Front. Immunol. 10, 208. https://doi.org/10.3389/fimmu.2019.00208.
Guilluy, C., Garcia-Mata, R., Burridge, K., 2011. Rho protein crosstalk: another social network? Trends Cell Biol. 21, 718–726. https://doi.org/10.1016/j.tcb.2011.08.002.
Hanna, S., El-Sibai, M., 2013. Signaling networks of Rho GTPases in cell motility. Cell. Signal. 25, 1955–1961. https://doi.org/10.1016/j.cellsig.2013.04.009.
Hanna, S., Miskolci, V., Cox, D., Hodgson, L., 2014. A new genetically encoded single-chain biosensor for Cdc42 based on FRET, useful for live-cell imaging. PLoS One 9. https://doi.org/10.1371/journal.pone.0096469.
He, F., Chen, Y., 2012. Wnt signaling in lip and palate development. Front. Oral Biol. https://doi.org/10.1159/000337619.
Herder, C., Swiercz, J.M., Müller, C., Peravali, R., Quiring, R., Offermanns, S., Wittbrodt, J., Loosli, F., 2013. ArhGEF18 regulates RhoA-Rock2 signaling to maintain neuro-epithelial apico-basal polarity and proliferation. Development 140, 2787–2797. https://doi.org/10.1242/dev.096487.
Hernández, S.E., Settleman, J., Koleske, A.J., 2004. Adhesion-dependent regulation of p190RhoGAP in the developing brain by the Abl-related gene tyrosine kinase. Curr. Biol. 14, 691–696. https://doi.org/10.1016/j.cub.2004.03.062.
Hoffmann, W., Schwarz, H., 1996. Ependymins: meningeal-derived extracellular matrix proteins at the blood-brain barrier. Int. Rev. Cytol. 165, 121–158. https://doi.org/10.1016/s0074-7696(08)62221-4.
Houweling, A.C., Gille, J.J.P., Baart, J.A., van Hagen, J.M., Lachmeijer, A.M., 2009. Variable phenotypic manifestation of IRF6 mutations in the Van der Woude syndrome and popliteal pterygium syndrome: implications for genetic counseling. Clin. Dysmorphol. 18, 225–227. https://doi.org/10.1097/MCD.0b013e32832d4a87.
Huber, C., Dias-Santagata, D., Glaser, A., O'Sullivan, J., Brauner, R., Wu, K., Xu, X., Pearce, K., Wang, R., Uzielli, M.L.G., Dagoneau, N., Chemaitilly, W., Superti-Furga, A., Dos Santos, H., Mégarbané, A., Morin, G., Gillessen-Kaesbach, G., Hennekam, R., der Burgt, I., Black, G.C.M., Clayton, P.E., Read, A., Le Merrer, M.,

Scambler, P.J., Munnich, A., Pan, Z.-Q., Winter, R., Cormier-Daire, V., 2005. Identification of mutations in CUL7 in 3-M syndrome. Nat. Genet. 37, 1119–1124. https://doi.org/10.1038/ng1628.

Huber, C., Delezoide, A.-L., Guimiot, F., Baumann, C., Malan, V., Le Merrer, M., Da Silva, D.B., Bonneau, D., Chatelain, P., Chu, C., Clark, R., Cox, H., Edery, P., Edouard, T., Fano, V., Gibson, K., Gillessen-Kaesbach, G., Giovannucci-Uzielli, M.-L., Graul-Neumann, L.M., van Hagen, J.-M., van Hest, L., Horovitz, D., Melki, J., Partsch, C.-J., Plauchu, H., Rajab, A., Rossi, M., Sillence, D., Steichen-Gersdorf, E., Stewart, H., Unger, S., Zenker, M., Munnich, A., Cormier-Daire, V., 2009. A large-scale mutation search reveals genetic heterogeneity in 3M syndrome. Eur. J. Hum. Genet. 17, 395–400. https://doi.org/10.1038/ejhg.2008.200.

Jaafar, L., Chamseddine, Z., El-Sibai, M., 2020. StarD13: a potential star target for tumor therapeutics. Hum. Cell 33, 437–443. https://doi.org/10.1007/s13577-020-00358-2.

Khalil, B.D., El-Sibai, M., 2012. Rho GTPases in primary brain tumor malignancy and invasion. J. Neuro-Oncol. 108, 333–339. https://doi.org/10.1007/s11060-012-0866-8.

Khalil, B.D., Hanna, S., Saykali, B.A., El-Sitt, S., Nasrallah, A., Marston, D., El-Sabban, M., Hahn, K.M., Symons, M., El-Sibai, M., 2014. The regulation of RhoA at focal adhesions by StarD13 is important for astrocytoma cell motility. Exp. Cell Res. 321, 109. https://doi.org/10.1016/j.yexcr.2013.11.023.

Kim, H.G., Herrick, S.R., Lemyre, E., Kishikawa, S., Salisz, J.A., Seminara, S., MacDonald, M.E., Bruns, G., Morton, C.C., Quade, B.J., Gusella, J.F., 2005. Hypogonadotropic hypogonadism and cleft lip and palate caused by a balanced translocation producing haploinsufficiency for FGFR1. J. Med. Genet. https://doi.org/10.1136/jmg.2004.026989.

Kunz, E., Rothammer, S., Pausch, H., Schwarzenbacher, H., Seefried, F.R., Matiasek, K., Seichter, D., Russ, I., Fries, R., Medugorac, I., 2016. Confirmation of a non-synonymous SNP in PNPLA8 as a candidate causal mutation for Weaver syndrome in Brown Swiss cattle. Genet. Sel. Evol. 48, 21. https://doi.org/10.1186/s12711-016-0201-5.

Lauffenburger, D.A., Horwitz, A.F., 1996. Cell migration: a physically integrated molecular process. Cell 84, 359–369. https://doi.org/10.1016/S0092-8674(00)81280-5.

Leslie, E.J., Marazita, M.L., 2013. Genetics of cleft lip and cleft palate. Am. J. Med. Genet. C Semin. Med. Genet. https://doi.org/10.1002/ajmg.c.31381.

Leslie, E.J., Mansilla, M.A., Biggs, L.C., Schuette, K., Bullard, S., Cooper, M., Dunnwald, M., Lidral, A.C., Marazita, M.L., Beaty, T.H., Murray, J.C., 2012. Expression and mutation analyses implicate ARHGAP29 as the etiologic gene for the cleft lip with or without cleft palate locus identified by genome-wide association on chromosome 1p22. Birth Defects Res. A Clin. Mol. Teratol. 94, 934–942. https://doi.org/10.1002/bdra.23076.

Lombardi, M.P., Bulk, S., Celli, J., Lampe, A., Gabbett, M.T., Ousager, L.B., van der Smagt, J.J., Soller, M., Stattin, E.L., Mannens, M.A.M.M., Smigiel, R., Hennekam, R. C., 2011. Mutation update for the PORCN gene. Hum. Mutat. https://doi.org/10.1002/humu.21505.

Nagata, K.-I., Inagaki, M., 2005. Cytoskeletal modification of Rho guanine nucleotide exchange factor activity: identification of a Rho guanine nucleotide exchange factor as a binding partner for Sept9b, a mammalian septin. Oncogene 24, 65–76. https://doi.org/10.1038/sj.onc.1208101.

Najm, P., El-Sibai, M., 2014. Palladin regulation of the actin structures needed for cancer invasion. Cell Adhes. Migr. 8, 29–35. https://doi.org/10.4161/cam.28024.

Nakajima, H., Tanoue, T., 2011. Lulu2 regulates the circumferential actomyosin tensile system in epithelial cells through p114RhoGEF. J. Cell Biol. 195, 245–261. https://doi.org/10.1083/jcb.201104118.

Nasrallah, A., Saykali, B., Al Dimassi, S., Khoury, N., Hanna, S., El-Sibai, M., 2014. Effect of StarD13 on colorectal cancer proliferation, motility and invasion. Oncol. Rep. 31, 505–515. https://doi.org/10.3892/or.2013.2861.

Niu, J., Profirovic, J., Pan, H., Vaiskunaite, R., Voyno-Yasenetskaya, T., 2003. G Protein betagamma subunits stimulate p114RhoGEF, a guanine nucleotide exchange factor for RhoA and Rac1: regulation of cell shape and reactive oxygen species production. Circ. Res. 93, 848–856. https://doi.org/10.1161/01.RES.0000097607.14733.0C.

Pertz, O., Hodgson, L., Klemke, R.L., Hahn, K.M., 2006. Spatiotemporal dynamics of RhoA activity in migrating cells. Nature 440, 1069–1072. https://doi.org/10.1038/nature04665.

Ravindran, E., Hu, H., Yuzwa, S.A., Hernandez-Miranda, L.R., Kraemer, N., Ninnemann, O., Musante, L., Boltshauser, E., Schindler, D., Hübner, A., Reinecker, H.-C., Ropers, H.-H., Birchmeier, C., Miller, F.D., Wienker, T.F., Hübner, C., Kaindl, A.M., 2017. Homozygous ARHGEF2 mutation causes intellectual disability and midbrain-hindbrain malformation. PLoS Genet. 13 https://doi.org/10.1371/journal.pgen.1006746.

Reynolds, K., Kumari, P., Rincon, L.S., Gu, R., Ji, Y., Kumar, S., Zhou, C.J., 2019. Wnt signaling in orofacial clefts: crosstalk, pathogenesis and models. DMM Dis. Model. Mech. https://doi.org/10.1242/dmm.037051.

Sadok, A., Marshall, C.J., 2014. Rho GTPases: masters of cell migration. Small GTPases 5. https://doi.org/10.4161/sgtp.29710.

Salloum, G., Jaafar, L., El-Sibai, M., 2020. Rho A and Rac1: antagonists moving forward. Tissue Cell 65, 101364. https://doi.org/10.1016/j.tice.2020.101364.

Saykali, B.A., El-Sibai, M., 2014. Invadopodia, regulation, and assembly in cancer cell invasion. Cell Commun. Adhes. 21, 207–212. https://doi.org/10.3109/15419061.2014.923845.

Setó-Salvia, N., Stanier, P., 2014. Genetics of cleft lip and/or cleft palate: association with other common anomalies. Eur. J. Med. Genet. 57, 381–393. https://doi.org/10.1016/j.ejmg.2014.04.003.

Shashoua, V.E., 1991. Ependymin, a brain extracellular glycoprotein, and CNS plasticity. Ann. N. Y. Acad. Sci. 627, 94–114. https://doi.org/10.1111/j.1749-6632.1991.tb25916.x.

Spiering, D., Hodgson, L., 2011. Dynamics of the Rho-family small GTPases in actin regulation and motility. Cell Adhes. Migr. 5, 170–180. https://doi.org/10.4161/cam.5.2.14403.

Terry, S.J., Zihni, C., Elbediwy, A., Vitiello, E., Leefa Chong San, I.V., Balda, M.S., Matter, K., 2011. Spatially restricted activation of RhoA signalling at epithelial junctions by p114RhoGEF drives junction formation and morphogenesis. Nat. Cell Biol. 13, 159–166. https://doi.org/10.1038/ncb2156.

Truong, A.B., Kretz, M., Ridky, T.W., Kimmel, R., Khavari, P.A., 2006. p63 regulates proliferation and differentiation of developmentally mature keratinocytes. Genes Dev. 20, 3185–3197. https://doi.org/10.1101/gad.1463206.

Wang, Y., Chen, C.-L., Iijima, M., 2011. Signaling mechanisms for chemotaxis. Develop. Growth Differ. 53, 495–502. https://doi.org/10.1111/j.1440-169X.2011.01265.x.

Wennerberg, K., Forget, M.-A., Ellerbroek, S.M., Arthur, W.T., Burridge, K., Settleman, J., Der, C.J., Hansen, S.H., 2003. Rnd proteins function as RhoA antagonists by activating p190 RhoGAP. Curr. Biol. 13, 1106–1115. https://doi.org/10.1016/s0960-9822(03)00418-4.

Zeiger, J.S., Beaty, T.H., Hetmanski, J.B., Wang, H., Scott, A.F., Kasch, L., Raymond, G., Jabs, E.W., VanderKolk, C., 2002. Genetic and environmental risk factors for sagittal craniosynostosis. J. Craniofac. Surg. 13, 602–606. https://doi.org/10.1097/00001665-200209000-00002.

Zhu, S., Liu, L., Korzh, V., Gong, Z., Low, B.C., 2006. RhoA acts downstream of Wnt5 and Wnt11 to regulate convergence and extension movements by involving effectors Rho kinase and diaphanous: use of zebrafish as an in vivo model for GTPase signaling. Cell. Signal. 18, 359–372. https://doi.org/10.1016/j.cellsig.2005.05.019.

Zohrabian, V.M., Forzani, B., Chau, Z., Murali, R., Jhanwar-Uniyal, M., 2009. Rho/ROCK and MAPK signaling pathways are involved in glioblastoma cell migration and proliferation. Anticancer Res. 29, 119–123.